Supporting Information

Andrews and Catalano 10.1073/pnas.1222820110

SI Text

Characterization of Mutant Terminase Enzymes. A number of mutations have been identified that affect the assembly of λ in vivo (1). Three were chosen for further study based on (*i*) their residual in vivo genome maturation activity and (*ii*) a significant defect in DNA packaging activity: gpA-K76R, gpA-T194M, and gpA-G212S. The three mutant enzymes were purified as terminase mix preparations using a published protocol (2). No significant differences were observed in the purification characteristics of the mutants relative to WT enzyme. The self-association behavior of the purified enzymes was characterized by sedimentation velocity analytical ultracentrifugation as described previously (2, 3). The T194M mutant terminase showed a significant assembly defect (Fig. S1) and was not considered further. The K76R and G212S mutant enzymes distributed between protomer and assembled tetramer species essentially identically to the WT enzyme (Fig. 2; Fig. S1); however, the G212S mutant showed residual DNA packaging activity in vivo, whereas the activity of K76R terminase was undetectable (1). Based on these observations, the K76R mutant terminase was chosen for use in these studies.

Genome Maturation Complex Model. The genome maturation data presented in Fig. 4 were analyzed using three separate models. All of the models presume that the catalytically competent complex positions two terminase protomers at the *cosN* site to introduce symmetric nicks into the duplex and then separate the strands (Fig. 1). The relative activity of the WT enzyme and that of K76R are taken as 1 and 1.7, respectively (Fig. 2*C*).

Model 1: Symmetric tetramer model. This model presumes that the maturation complex is composed of four protomers and that incorporation of a mutant protomer into any of the four positions has an equivalent effect on the reaction. The normalized activity for each of the individual chimeric motors is presented in Fig. S3 and was used in Eq. **3** to calculate the ensemble activity in solution. The predicted ensemble activity assuming zero (C = 0, blue line), 50% (C = 0.5, purple line), or 100% (C = 1, red line) coordination is displayed in Fig. 4. The sum of squared error (SSE) for each model is presented at the bottom of Fig. S3.

Model 2: Symmetric dimer model. This model presumes that the maturation complex is structurally distinct from the tetrameric packaging motor and is composed of a simple dimer of protomers bound at *cosN* ($n = 2$; Fig. S4*A*). The normalized activity for each of the individual chimeric motors is presented in Fig. S4*B* and was used in Eq. **3** to calculate the ensemble activity in solution. The predicted ensemble activity assuming 100% (C = 1) coordination is displayed as a black dotted line in Fig. 4. A model that assumes limited coordination between the protomers (C = 0) poorly describes the data (superimposable and indistinguishable from the blue line in Fig. 4). The SSE for each model is displayed at the bottom of Fig. S4*B*.

Model 3: Tetramer model with "half-site" activity. This model assumes that the maturation complex is a tetramer composed of a dimer of dimers and that only one of the dimers is required for strand separation activity; the second dimer is required for efficient assembly at *cos* but is catalytically silent (Fig. S5*A*) (2). The ensemble distribution as a function of *k* is displayed in Fig. S5*B*. We initially considered a model with strong coordination (C = 1) between the protomers bound at *cosN* and that incorporation of a WT protomer limits the reaction. Thus, WT–WT homodimers (blue–blue) and WT–K76R heterodimers (blue–red) possess a relative activity of 1, whereas the K76R–K76R mutant homodimer (red–red) possesses a relative activity of 1.7 (Fig. S5*B*). The calculated activities of the individual motors were used to calculate the ensemble activity according to Eq. **3**. The predicted activity as a function of *f* is shown as a green line in Fig. 4, which describes the data well. We also considered a dimer of dimers model with no coordination between the two protomers bound to *cosN* (C = 0), but this yielded a poor fit to the data (superimposable and indistinguishable from the blue line in Fig. 4).

Construction of a λ TerL Structural Homology Model. High-resolution structural data on λ terminase are limited to the DNA binding domain of the TerS (gpNu1) subunit. Crystal structures of the motor domain and full-length TerL from bacteriophage T4 have been published (4, 5). We generated a structural homology model for the λ TerL subunit using the iTASSER search engine (http://zhanglab.ccmb.med.umich.edu/I-TASSER/) with gpA as the query sequence. iTasser returned the phage T4 TerL subunit (RCSB PDB #3CPE) as a top structural homology candidate, and the resulting structure is displayed in Fig. S6.

1. Duffy C, Feiss M (2002) The large subunit of bacteriophage lambda's terminase plays a role in DNA translocation and packaging termination. *J Mol Biol* 316(3):547–561.
2. Andrews BT, Catalano CE (2012) The enzymology of a viral genome packaging motor is influenced by the assembly state of the motor subunits. *Biochemistry* 51(46): 9342–9353.
3. Maluf NK, Yang Q, Catalano CE (2005) Self-association properties of the bacteriophage lambda terminase holoenzyme: Implications for the DNA packaging motor. *J Mol Biol* 347(3):523–542.
4. Sun S, Kondabagil K, Gentz PM, Rossmann MG, Rao VB (2007) The structure of the ATPase that powers DNA packaging into bacteriophage T4 procapsids. *Mol Cell* 25(6): 943–949.
5. Sun S, et al. (2008) The structure of the phage T4 DNA packaging motor suggests a mechanism dependent on electrostatic forces. *Cell* 135(7):1251–1262.

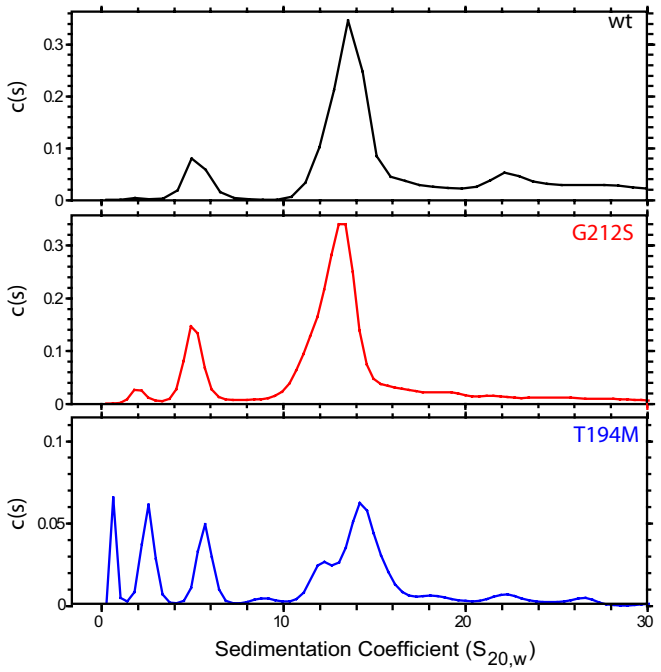

Fig. S1. Self-association behavior of WT and mutant terminase enzymes. The indicated enzymes were purified as terminase mix preparations, and their hydrodynamic behavior was analyzed as previously described (2, 3).

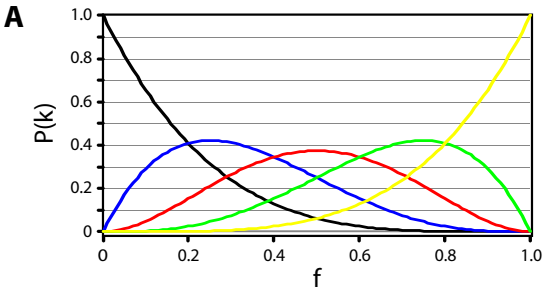

B A(k) (Normalized Packaging Activity)

Motor (n=4)	C=0	C=1	C=0.9	C=0.8
k=0	1.0	1.0	1.0	1.0
k=1	0.75	0	0.68	0.6
k=2	0.5	0	0.45	0.4
k=3	0.25	0	0.23	0.2
k=4	0	0	0	0
SSE=	$9.21\text{x}10^{-1}$	$4.55\text{x}10^{-3}$	$1.98\text{ex}10^{-2}$	$5.10\text{x}10^{-2}$

Fig. S2. The DNA packaging model. (*A*) Binomial distribution of chimeric motors as a function of *f*. The data were generated from Eq. 2 assuming a tetrameric motor (n= 4) and k = 0 (black), 1 (blue), 2 (red), 3 (green), and 4 (yellow). (*B*) Calculated activity of individual tetrameric motors containing *k* mutant protomers. WT and K76R mutant protomers are depicted in blue and red, respectively. A_{WT} and A_{MT} equal 1 and 0, respectively (Fig. 2*C*). The model presumes a symmetric complex and that incorporation of a mutant protomer into any of the four positions has an equivalent effect. The normalized packaging activities were used to determine the activities of chimeric motors using Eq. **3**, and data are displayed in Fig. 3. The SSE for each model is presented at the bottom of the table.

A(k) (Normalized Separation Activity)

Motor (n=4)	C=0	C=1	C=0.5	Dimer of Dimers
k=0	1.0	1.0	1.0	1.0
k=1	1.18	1.0	1.09	1.0
k=2	1.35	1.0	1.18	1.12
k=3	1.53	1.0	1.26	1.35
k=4	1.7	1.7	1.7	1.7
SSE=	2.84×10^{-2}	2.51×10^{-2}	2.99×10^{-3}	5.65×10^{-4}

Fig. S3. Symmetric tetramer model activity. Calculated activity of individual tetrameric maturation complexes containing *k* mutant protomers. WT and K76R mutant protomers are depicted in blue and red, respectively. A_{WT} and A_{MT} equal 1 and 1.7, respectively (Fig. 2*C*).

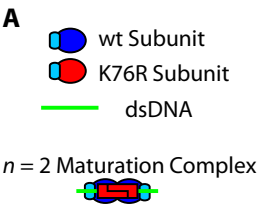

B

Motor (n=2)	C=0	C=1
k=0	1.0	1.0
k=1	1.35	1.0
k=2	1.7	1.7
SSE=	2.75×10^{-2}	5.71×10^{-4}

Fig. S4. Symmetric dimer model. (*A*) Symmetric dimer model for the genome maturation complex. WT and K76R mutant protomers are depicted in blue and red, respectively. DNA is depicted as a green line. Two terminase protomers assemble at *cos* to engender the catalytically competent maturation complex. (*B*) Calculated activity of individual dimeric motors containing *k* mutant protomers and relevant SSE.

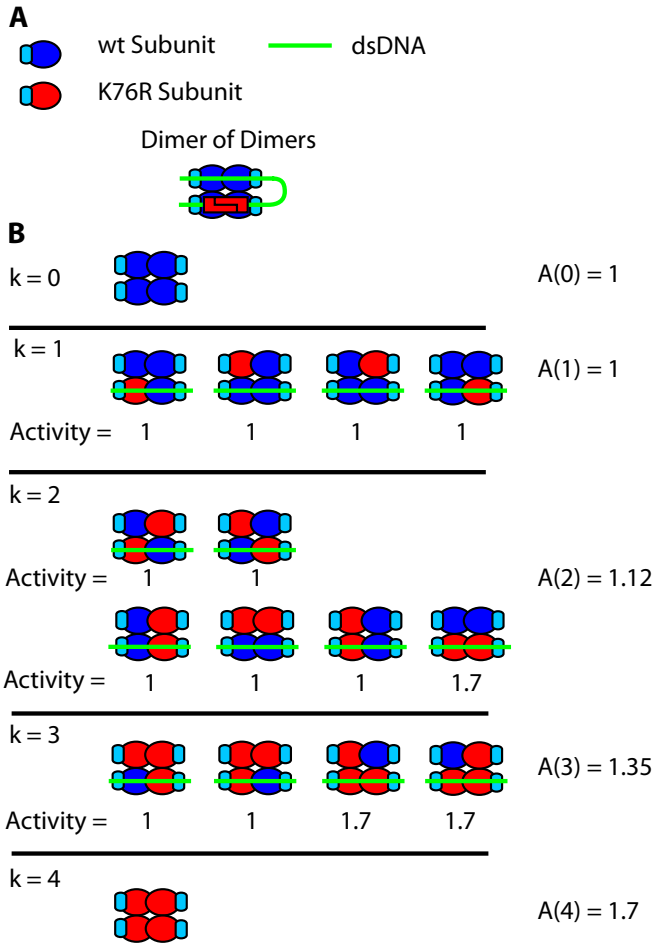

Fig. S5. Dimer of dimer model. (*A*) The maturation complex is composed of a dimer of protomer dimers. A catalytically competent dimer binds to *cosN* (green line) to nick and then separate the strands; the second dimer is required for optimal activity but is catalytically silent (half-site activity). (*B*) Ensemble distribution of chimeric motors in a dimer of dimers maturation complex. WT and K76R mutant protomers are depicted in blue and red, respectively. DNA is depicted as bound only to the catalytically active dimer for clarity. *k* represents the number of mutant protomers assembled into the complex; the calculated activity of individual motors containing *k* mutant protomers and assuming tight coordination between subunits in the catalytically competent dimer (C = 1) is indicated beneath each complex. A_{WT} and A_{MT} equal 1 and 1.7, respectively (Fig. 2*C*). Values of $A(k)$ are also reported in Fig. S3 with corresponding SSE.

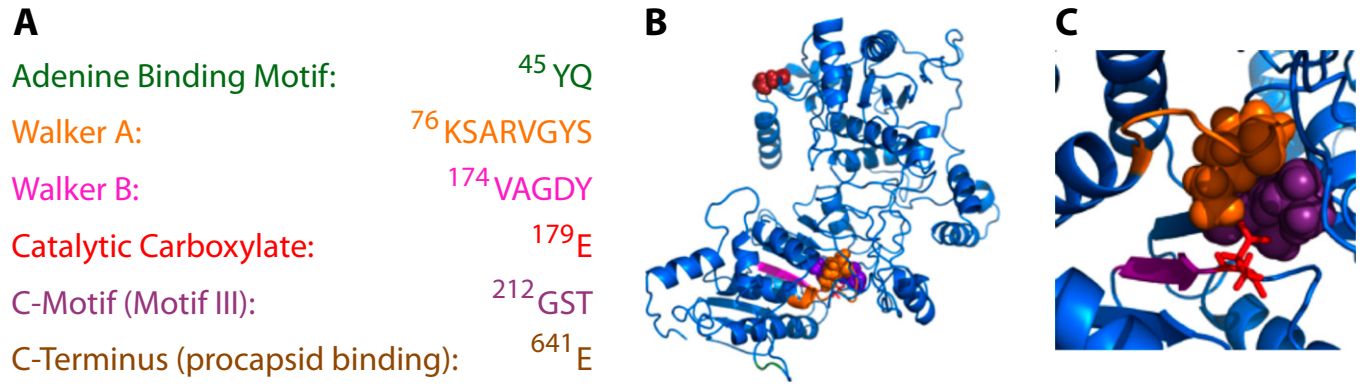

Fig. S6. Structural homology model for the λ TerL subunit. (*A*) The conserved sequence motifs identified in the motor domains of terminase and SF2 helicase enzymes are shown for the λ TerL subunit. (*B*) Structural homology model for λ TerL with conserved motifs colored as in *A*. Lys76, C-motif residues, and the C terminus (E641, which is implicated in procapsid binding) are displayed as spheres. The catalytic carboxylate is displayed as sticks. (*C*) Expanded view showing K76 and the C-motif residues as orange and purple spheres, respectively, and the catalytic carboxylate as red sticks.